



# Proteomic mapping by rapamycin-dependent targeting of APEX2 identifies binding partners of VAPB at the inner nuclear membrane

Received for publication, December 22, 2018, and in revised form, August 5, 2019. Published, Papers in Press, September 13, 2019, DOI 10.1074/jbc.RA118.007283

Christina James<sup>‡</sup>, Marret Müller<sup>‡</sup>,  Martin W. Goldberg<sup>§</sup>, Christof Lenz<sup>¶||</sup>, Henning Urlaub<sup>¶||</sup>, and  Ralph H. Kehlenbach<sup>‡1</sup>

From the <sup>‡</sup>Department of Molecular Biology, Faculty of Medicine, Göttingen Center for Molecular Biosciences (GZMB), Georg August University Göttingen, Humboldtallee 23, 37073 Göttingen, Germany, <sup>§</sup>School of Biological and Biomedical Sciences, Durham University, Durham DH1 3LE, United Kingdom, <sup>¶</sup>Bioanalytics Group, Institute of Clinical Chemistry, University Medical Center Göttingen, Robert-Koch-Strasse 40, 37075 Göttingen, Germany, and <sup>||</sup>Bioanalytical Mass Spectrometry Group, Max Planck Institute for Biophysical Chemistry, Am Fassberg 11, 37077 Göttingen, Germany

Edited by John M. Denu

Vesicle-associated membrane protein-associated protein B (VAPB) is a tail-anchored protein that is present at several contact sites of the endoplasmic reticulum (ER). We now show by immunoelectron microscopy that VAPB also localizes to the inner nuclear membrane (INM). Using a modified enhanced ascorbate peroxidase 2 (APEX2) approach with rapamycin-dependent targeting of the peroxidase to a protein of interest, we searched for proteins that are in close proximity to VAPB, particularly at the INM. In combination with stable isotope labeling with amino acids in cell culture (SILAC), we confirmed many well-known interaction partners at the level of the ER with a clear distinction between specific and nonspecific hits. Furthermore, we identified emerin, TMEM43, and ELYS as potential interaction partners of VAPB at the INM and the nuclear pore complex, respectively.

The family of vesicle-associated membrane protein (VAMP/synaptobrevin)-associated proteins (VAPs)<sup>2</sup> includes VAPA

This work was supported by Deutsche Forschungsgemeinschaft Grant SFB1190 (to R. H. K. and H. U.). The authors declare that they have no conflicts of interest with the contents of this article.

This article contains Figs. S1–S3 and Tables S1–S4.

The mass spectrometric raw data and spectral libraries associated with this manuscript are available from ProteomeXchange with the accession number PXD012157.

<sup>1</sup> To whom correspondence should be addressed. Tel.: 49-551-395950; Fax: 49-551-395960; E-mail: rkehlen@gwdg.de.

<sup>2</sup> The abbreviations used are: VAP, vesicle-associated membrane protein (VAMP/synaptobrevin)-associated protein; ER, endoplasmic reticulum; INM, inner nuclear membrane; APEX, ascorbate peroxidase; SILAC, stable isotope labeling with amino acids in cell culture; ELYS, embryonic large molecule derived from yolk sac; ACBD5, acyl-CoA-binding domain protein 5; PTPIP51, tyrosine phosphatase-interacting protein 51; OSBP, oxysterol-binding protein; FFAT, two phenylalanines in an acidic tract; BioID, biotin identification; HRP, horseradish peroxidase; dGFP, double GFP; GST, glutathione S-transferase; NLS, nuclear localization signal; FKBP12, 12-kDa FK506-binding protein; FRB, FKBP-rapamycin-binding; RAPIDS, rapamycin- and APEX-dependent identification of proteins by SILAC; HA, hemagglutinin; GAPDH, glyceraldehyde-3-phosphate dehydrogenase; ARID4A, AT-rich interactive domain-containing protein 4 A; LAP, lamina-associated polypeptide; TOR1AIP1, Torsin-1A-interacting protein 1; TMPO, thymopoietin; NPC, nuclear pore complex; DSP, dithiobis(succinimidyl propionate); PLA, proximity ligation assay; Bis-Tris, 2-[bis(2-hydroxyethyl)amino]-2-(hydroxymethyl)propane-1,3-diol; DAPI, 4',6-diamidino-2-phenylindole.

and VAPB with described roles in the morphology and function of the endoplasmic reticulum (ER) and Golgi apparatus (1, 2). VAPB is a tail-anchored protein, *i.e.* a protein containing a single transmembrane domain close to its C terminus. Such proteins are typically inserted into the cellular membrane system in a post-translational manner (3, 4). In its N-terminal region, VAPB contains a characteristic major sperm protein domain. VAPB localizes largely to the ER, and its binding to several partner proteins has been shown to mediate the association of the ER with other organelles. Acyl-CoA-binding domain protein 5 (ACBD5), for example, interacts with VAPB and is involved in binding peroxisomes to the ER (5), whereas tyrosine phosphatase-interacting protein 51 (PTPIP51) and VAPB form an ER-mitochondria tethering complex (6). In the secretory pathway, VAPB interacts with the Yip1-interacting factor homologue YIF1A, *e.g.* at the level of the ER-Golgi intermediate compartment (7). Furthermore, several oxysterol-binding proteins (OSBPs), which play important roles in lipid transport, interact with VAPB (8), and Kv2 potassium channels form ER-plasma membrane junctions via interactions with VAPB (9). In total, >100 proteins have been reported to directly or indirectly interact with VAPB and/or the highly similar protein VAPA (10, 11) (see also <https://thebiogrid.org>).<sup>3</sup> A major binding motif, which is found in many VAPB-interacting proteins, is the “two phenylalanines in an acidic tract” (FFAT) motif (11, 12). Typically, the FFAT (or FFAT-like) motif interacts with the major sperm protein domain of VAPB. One example of a protein containing the FFAT motif that binds VAPB is the WD repeat-containing protein WDR44 (13). A mutation in VAPB (P56S) is involved in an autosomal dominant form of amyotrophic lateral sclerosis (ALS) (14) and blocks transport of nucleoporins and emerin, a major protein of the inner nuclear membrane (INM), to the nuclear envelope (15).

Several methods have been developed for the identification of proteins that are in close proximity to each other. They typically introduce biotin into unknown proteins as a tag that can be used for affinity capture with immobilized streptavidin and

<sup>3</sup> Please note that the JBC is not responsible for the long-term archiving and maintenance of this site or any other third party-hosted site.

## Binding partners of VAPB at the inner nuclear membrane

subsequent analysis by MS (for reviews, see Refs. 16 and 17). One prominent approach, proximity-dependent biotin identification (BioID), is based on a mutant form of the biotin ligase BirA, which can be fused to a protein of interest (the bait) whose neighboring proteins are to be analyzed (18). The enzyme part of the fusion protein releases reactive biotin, which can modify proteins (the prey) within a small spatial range. One drawback of this method is a rather long reaction time of >15 h, although a faster method has been described very recently (19). As an alternative to biotin ligase-dependent modifications, peroxidase-based methods have been introduced that allow short reaction times in the range of seconds to minutes (20). Ascorbate peroxidase (APEX) is a plant enzyme that generates biotin-phenoxy radicals from biotin phenol in the presence of H<sub>2</sub>O<sub>2</sub>. These radicals have a very short half-life and, thus, can modify proteins within a range of ~20 nm, reacting with several amino acids with tyrosine as the primary site of biotinylation (21). Importantly, APEX can be fused to the N or C terminus of proteins and may also reside internally. Furthermore, the enzyme has been shown to be active in several cellular compartments (20, 22, 23). Recently, APEX2, which is far more active than the original enzyme, was introduced (24). So far, APEX- or APEX2-based methods have mainly been used for the identification of proteins that reside in defined subcellular compartments, e.g. in primary cilia (23) or in the intermembrane space of mitochondria (25). As an alternative to APEX, horseradish peroxidase (HRP) can also be used as an enzyme to initiate the formation of biotin-phenoxy radicals, and antibody-directed targeting of HRP to proteins of interest was recently described (26).

We previously characterized the post-translational insertion mechanisms of emerin into ER membranes and analyzed targeting of the protein to the INM (27). For this, we applied a rapamycin-dependent dimerization method to monitor sequestration of a soluble nuclear reporter protein (dGFP-GST-NLS-FKBP12) to mCherry-tagged emerin (mCherry-FRB-emerin) at the INM. In this system, rapamycin binds to its two cognate binding regions, a 12-kDa FK506-binding protein (FKBP12) and an FKBP-rapamycin-binding (FRB) cassette, promoting rapid interaction of the appropriately tagged proteins (28).

We now combine the APEX2 technology with the rapamycin-dependent dimerization approach. To this end, we target FKBP12-tagged APEX2 to FRB-tagged proteins in a rapamycin-dependent manner. SILAC, followed by quantitative MS, then allows the comparison of proteins that are biotinylated by APEX2 in either the absence or presence of rapamycin. Using this method (rapamycin- and APEX-dependent identification of proteins by SILAC or RAPIDS), we found RMDN3 (PTPIP51), ACBD5, YIF1A, OSBPL9, and other previously known interacting proteins of VAPB. Using a version of APEX2 that accumulates in the nucleus, we identified additional neighboring proteins of VAPB that reside at the nuclear envelope, e.g. emerin, TMEM43, lamins, and the nucleoporin embryonic large molecule derived from yolk sac (ELYS; AHCTF1). We further demonstrated the INM localization of VAPB by immunoelectron microscopy and confirmed the close proximity of endogenous VAPB with several of the newly identified proteins

using proximity ligation assays and coimmunoprecipitation experiments.

## Results

### VAPB resides at the INM

VAPB is typically described as an ER-resident protein, mediating interactions with multiple organelles. In addition, VAPB seems to play a role in the dynamics of the nuclear envelope and nuclear pore complex. In this context, it was reported to affect transport of emerin to the INM (15). A localization of VAPB itself to the INM, however, has not been demonstrated so far. We therefore investigated the subcellular localization of VAPB in detail. We first analyzed endogenous VAPB by indirect immunofluorescence using different buffers for the procedure. The specificity of the anti-VAPB antibody was confirmed by siRNA-mediated knockdown (see Fig. 6). As shown before, VAPB localized to the ER, with a clear rim around the nucleus visible in many cells (Fig. 1A). Interestingly, the ratio of the ER and the nuclear envelope signal varied a lot, depending on the buffer used (Fig. 1A, compare panels *i* and *ii*). Similar to the endogenous protein, differently tagged versions of VAPB (mCherry-FRB-VAPB and HA-FRB-VAPB) were also found at the level of the ER and the nuclear envelope (Fig. 1B). We next tested whether the nuclear rim could reflect targeting of VAPB not only to the outer but also to the inner nuclear membrane. For readout, we used our established rapamycin system (27). As shown before for emerin, the nuclear reporter protein dGFP-GST-NLS-FKBP12 was sequestered to the nuclear rim upon the addition of rapamycin in cells coexpressing mCherry-FRB-VAPB (Fig. 1C). This result suggested that at least a portion of the exogenously expressed VAPB reached the INM. To unequivocally demonstrate INM localization of endogenous VAPB, we performed immunoelectron microscopy. As shown in Fig. 1D, immunoreactivity was detected at mitochondria, possibly reflecting the interaction of VAPB with PTPIP51. Furthermore, a significant number of gold dots were found at the level of the INM and in close proximity to nuclear pores. In addition to these morphological studies, we also performed biochemical analyses. Obtaining pure INM fractions is hardly possible; nevertheless, we subjected cell lysates to an established fractionation protocol (29). As shown in Fig. S1, VAPB was largely recovered in the same fraction as emerin and other proteins of the nuclear envelope, although other membrane proteins are certainly expected in this fraction as well. Together, our results clearly point to a localization of a fraction of the cellular VAPB pool at the INM. These results are in line with a recent study, published during the review process of this paper, that suggests a role of VAPB in nuclear egress of herpes simplex viral particles (30).

### APEX2-dependent biotinylation of proteins

A number of membrane proteins exposing binding regions to the cytoplasm have been shown to interact with the ER form of VAPB (2). A portion of VAPB, however, localizes to the INM, so we then set out to devise a method for the identification of neighboring partners of VAPB that allows focus on either the cytoplasm (where the majority of VAPB is expected) or the nuclear compartment. Our approach is based on the APEX2

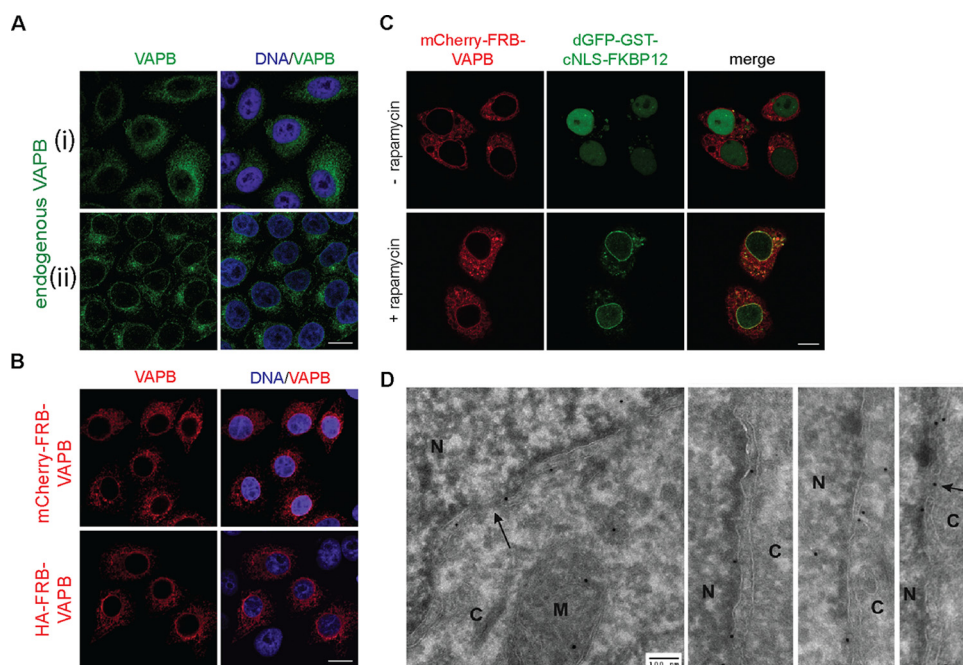


**Figure 1. VAPB localizes to the INM.** *A*, HeLa cells were grown on coverslips and subjected to indirect immunofluorescence using antibodies against VAPB. Cells were blocked with 3% BSA (*panel i*) or with Sigma Duolink blocking solution (*panel ii*). *B*, HeLa cells were transfected with plasmids coding for mCherry-FRB-VAPB or HA-FRB-VAPB as indicated. *C*, HeLa cells were cotransfected with plasmids coding for mCherry-FRB-VAPB and dGFP-GST-cNLS-FKBP12. After treatment with (+) or without (–) rapamycin, cells were fixed and analyzed by confocal microscopy. Scale bars, 10  $\mu$ m. *D*, HeLa cells were analyzed by immunoelectron microscopy using antibodies against VAPB. *C*, cytoplasm; *M*, mitochondria; *N*, nucleus. The arrows indicate nuclear pore complexes. Scale bar, 100 nm.

method for identification of proximity partners. In a “classic” approach, we first fused APEX2 directly to VAPB (Fig. 2*A*, left), as done before for many other proteins (9, 20–23, 25, 31–35). HeLa cells were transfected with constructs coding for APEX2-VAPB or, for a control reaction, GFP-APEX2. Fig. 2*B* shows the subcellular localization of the APEX2 fusion proteins: as expected, GFP-APEX2 is found all over the cell and should promote unspecific biotinylation of many cellular proteins, whereas APEX2-VAPB localizes largely to the ER, very similarly to other fusion proteins of VAPB (compare Fig. 1*B*). Next, the cells were subjected to the biotinylation protocol, including loading of cells with biotin-phenol and a short pulse with H<sub>2</sub>O<sub>2</sub>. For analysis, biotinylated proteins were enriched using neutravidin beads and detected by Western blotting. As shown in Fig. 2*C*, both fusion proteins were detected at similar levels in total cell lysates and in the protein fractions as bound to the neutravidin beads, indicating self-biotinylation. Furthermore, they led to a similar pattern of biotinylated proteins as detected by streptavidin-HRP. Next, we probed the blots with antibodies against proteins that had previously been identified as interaction partners of VAPB. Indeed, ACBD5 and OSBPL9 were clearly enriched when cells expressed APEX2-VAPB. In the control cells expressing GFP-APEX2, much lower levels of ACBD5 and OSBPL9 were detected (Fig. 2*C*, compare lanes 7 and 8). This result shows that the APEX method is suited for the identification of interaction/proximity partners of VAPB at the level of the ER. We noted, however, that the difference between specific and unspecific biotinylation (*i.e.* modification in cells expressing APEX2-VAPB *versus* cells expressing GFP-APEX2) varied a lot, possibly resulting from different transfection efficiencies. We therefore modified our approach in a way that

should allow a better control over specific *versus* unspecific biotinylation and combined APEX2-dependent biotinylation with the protocol for rapamycin-dependent targeting of proteins to a protein of interest (27). For a first proof of principle, we constructed a GFP-linked version of APEX2 with the rapamycin-interaction cassette FKBP12 (Fig. 2*A*, right). Cells were transfected with this construct together with a construct coding for mCherry-FRB-VAPB. Transfected cells were treated with or without rapamycin and subjected to the biotinylation protocol. Fig. 2*B* shows the localization of mCherry-FRB-VAPB at the ER and the nuclear envelope and the recruitment of GFP-FKBP12-APEX2 to these sites upon addition of rapamycin. This treatment resulted in a pronounced overlap of the GFP and mCherry signals, suggesting a tight interaction of FKBP12-GFP-APEX2 with mCherry-FRB-VAPB (compare Fig. 1*C*). As for the classic approach, cells were then subjected to the biotinylation protocol, and biotinylated proteins were analyzed by Western blotting. As shown in Fig. 2*C*, ACBD5 and OSBPL9 were detected as biotinylated proteins (*i.e.* in the bound fraction) when cells had been treated with the drug, indicating rapamycin-dependent targeting of APEX2 to mCherry-FRB-VAPB and biotinylation of the known VAPB interaction partners. The levels of proteins that were recovered from the neutravidin beads were as high or higher than those found in the classic experiment using APEX2-VAPB as a fusion protein (Fig. 2*C*, compare lanes 4 and 8; also compare with Fig. 3*C*). The added advantage of rapamycin-dependent targeting of APEX2 to our protein of interest, however, is 2-fold. First, a simple, single-parameter-change experiment ( $\pm$ rapamycin) can be performed for subsequent analysis of biotinylated proteins by quantitative MS and discrimination between specific and

## Binding partners of VAPB at the inner nuclear membrane

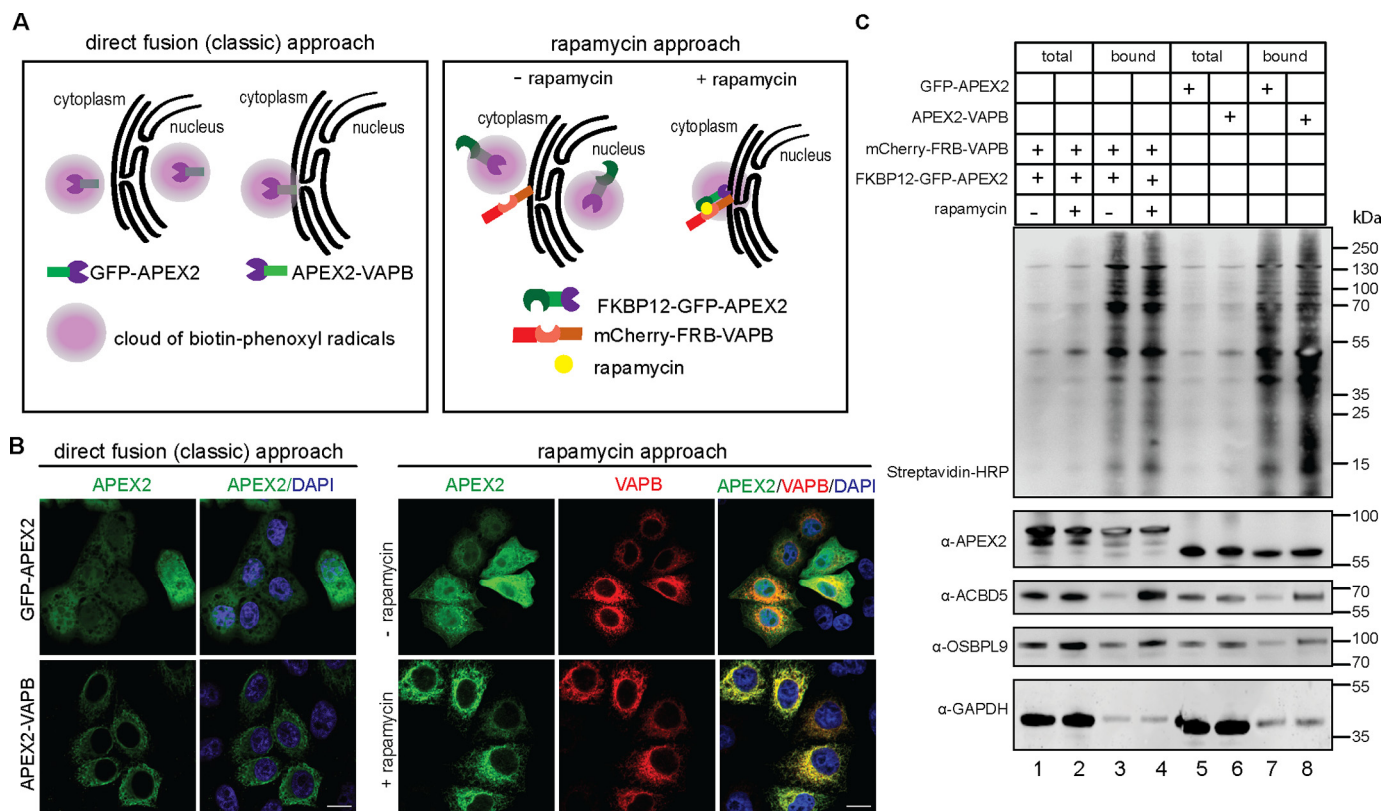


**Figure 2. Comparison of the classic and a new APEX approach.** *A*, schemes of the “direct fusion (classic) approach” (*left*) and the “rapamycin (new) approach” (*right*). *B*, for the direct fusion and rapamycin approaches, cells were transfected with plasmids coding for GFP-APEX2 or APEX2-VAPB and FKBP12-GFP-APEX2 and mCherry-FRB-VAPB, respectively. Cells were analyzed directly (*left*) or upon incubation with or without rapamycin (*right*). Scale bars, 10  $\mu$ m. *C*, cells were transfected as in *B* and subjected to the biotinylation protocol. Biotinylated proteins were enriched using neutravidin beads, and total and bound proteins were analyzed by SDS-PAGE followed by Western blotting. Note that GFP-APEX2 (*lanes 5 and 7*) and APEX2-VAPB (*lanes 6 and 8*) have very similar molecular weights.

unspecific hits. Second, the physical separation of APEX2 from the protein of interest allows an independent subcellular localization of the enzyme and, hence, a control over the population of cellular proteins that are potential targets for biotinylation. This is of particular importance for proteins like VAPB that can engage in interactions with different sets of proteins residing at distinct localizations.

### RAPIDS

Based on the results described above, we decided to use the combined APEX2/rapamycin system for the identification of novel VAPB proximity partners. The outline for an experiment with a version of APEX2 with the rapamycin-interaction cassette and identification of proteins by SILAC and quantitative MS is depicted in Fig. 3A. Briefly, cells are grown in media containing either light or heavy isotopes of the amino acids lysine and arginine and transfected with plasmids coding for mCherry-FRB-VAPB and FKBP12-GFP-APEX2. The two types of cells (“light” and “heavy”) are then treated with or without rapamycin and subjected to the biotinylation procedure. Cellular lysates are combined, and biotinylated proteins are enriched by binding to neutravidin beads. Mass spectrometry of eluted proteins then allows a direct comparison between +rapamycin (*i.e.* specific biotinylation close to mCherry-FRB-VAPB) and –rapamycin (*i.e.* background biotinylation) conditions. A quantitative evaluation of heavy and light tryptic fragments of biotinylated proteins should immediately yield proteins that were in

close proximity to mCherry-FRB-VAPB in the presence of rapamycin. Fig. S2A shows the controls for H<sub>2</sub>O<sub>2</sub>-dependent protein biotinylation. Prominent bands that are seen in the absence of H<sub>2</sub>O<sub>2</sub> correspond to endogenously biotinylated proteins. Similar transfection efficiencies in the two sets of cells (light and heavy) are controlled in Fig. S2B.

Fig. 3B shows the combined results of two independent experiments, each with forward (*i.e.* using light and heavy media for the +rapamycin and –rapamycin conditions) and reverse reactions (*i.e.* with changed conditions, as depicted in Fig. 3A). Proteins that are preferentially biotinylated in the presence of rapamycin in both forward (*x axis*) and reverse reactions (*y axis*) are expected in the *upper left quadrant* of the plot. One prominent protein here is VAPB itself, indicating its modification by the APEX2 fusion protein. Many previously known cytoplasmic interaction partners of VAPB were also identified with high levels of significance, including PTPIP51 (RMDN3), YIF1A, WDR44, OSBPL9, OSBPL8, and ACBD5. GAPDH, by contrast, was found in the cloud of proteins that were hardly affected by rapamycin, close to the *intersection* of the *x* and *y axes*. The list of identified proteins is presented in Table S1. Interestingly, the INM protein emerin was also identified with a high significance. Another potential interaction partner is TMEM43, also known as LUMA, a membrane protein that interacts with emerin at the INM (36) and plays a role in certain forms of muscular dystrophies (37). Its localization,

## Binding partners of VAPB at the inner nuclear membrane

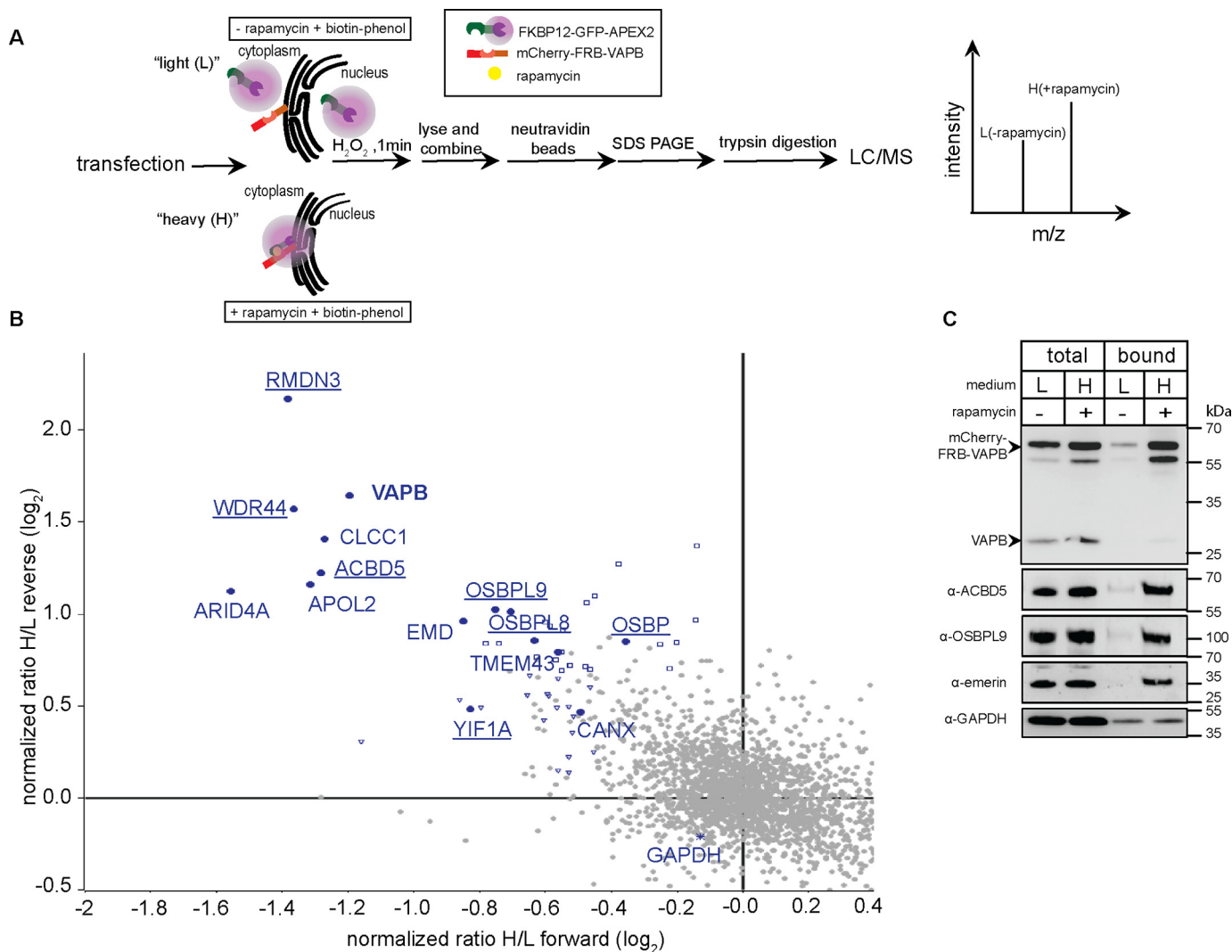


**Figure 3. Proximity mapping of mCherry-FRB-VAPB by RAPIDS.** *A*, experimental workflow. Cells grown in light or heavy medium are cotransfected with plasmids coding for FKBP12-GFP-APEX2 and mCherry-FRB-VAPB and subjected to APEX2-dependent biotinylation in the absence or presence of rapamycin. Note that this labeling scheme reflects the reverse reaction. In the forward reaction, light and heavy media are used for cells treated with or without rapamycin, respectively. Proteins from cell lysates are bound to neutravidin beads, and the total and bound fractions are analyzed by LC-MS. *B*, the scatter plot resulting from two independent experiments shows normalized  $\log_2$  ratios of proteins eluted from neutravidin beads in forward (heavy medium (*H*) without rapamycin; light medium (*L*), with rapamycin; *x* axis) and reverse (heavy medium, with rapamycin; light medium, without rapamycin; *y* axis) experiments. The plot focuses on the upper left quadrant because in the forward reaction, low heavy/light ratios (i.e. negative  $\log_2$  values) are expected for specific hits, whereas high ratios are expected in the reverse reaction. Known interacting partners of VAPB are underlined. Closed circles, proteins that were significant in all experiments; open triangles, proteins that were significant only in forward experiments; open squares, proteins that were significant only in reverse experiments. *C*, total cell lysates (*total*) and proteins bound to neutravidin beads (*bound*) from one of the experiments depicted in *B* were analyzed by Western blotting using antibodies against VAPB, ACBD5, OSBPL9, emerin, and GAPDH as a loading control.

however, is controversial because it was mainly found in zonula adherens and punctum adherens plaques in another study (38). Another nuclear protein that was identified is the AT-rich interactive domain-containing protein 4 A (ARID4A). This protein, also known as Rbbp1, is a retinoblastoma-binding protein (39) with functions in chromatin remodeling (40). The significance of the proximity and/or interaction of VAPB and ARID4A remains to be investigated.

Next, we performed Western blotting to confirm the MS data. As shown in Fig. 3C, high levels of mCherry-FRB-VAPB, ACBD5, OSBPL9, and emerin were detected in the bound fraction when the cells had been treated with rapamycin, confirming rapamycin-dependent biotinylation. For GAPDH, by contrast, very similar levels were observed for rapamycin-treated

and nontreated cells. Based on the successful identification of known interaction partners, we termed our approach “RAPID SILAC” or “RAPIDS.”

### RAPIDS using a nuclear version of APEX2

The identification of emerin supported the notion that VAPB can reach the INM (see Fig. 1), although emerin could also localize to other regions of the cell (41, 42). Two parameters of the assay as performed above disfavor the identification of *bona fide* INM proteins. First, FKBP12-GFP-APEX2 is found all over the cell and may preferentially interact with VAPB that localizes to the ER upon addition of rapamycin. Second, the version of VAPB in this experiment contains a large cytoplasmic mCherry tag. Although the protein can reach the INM to

## Binding partners of VAPB at the inner nuclear membrane

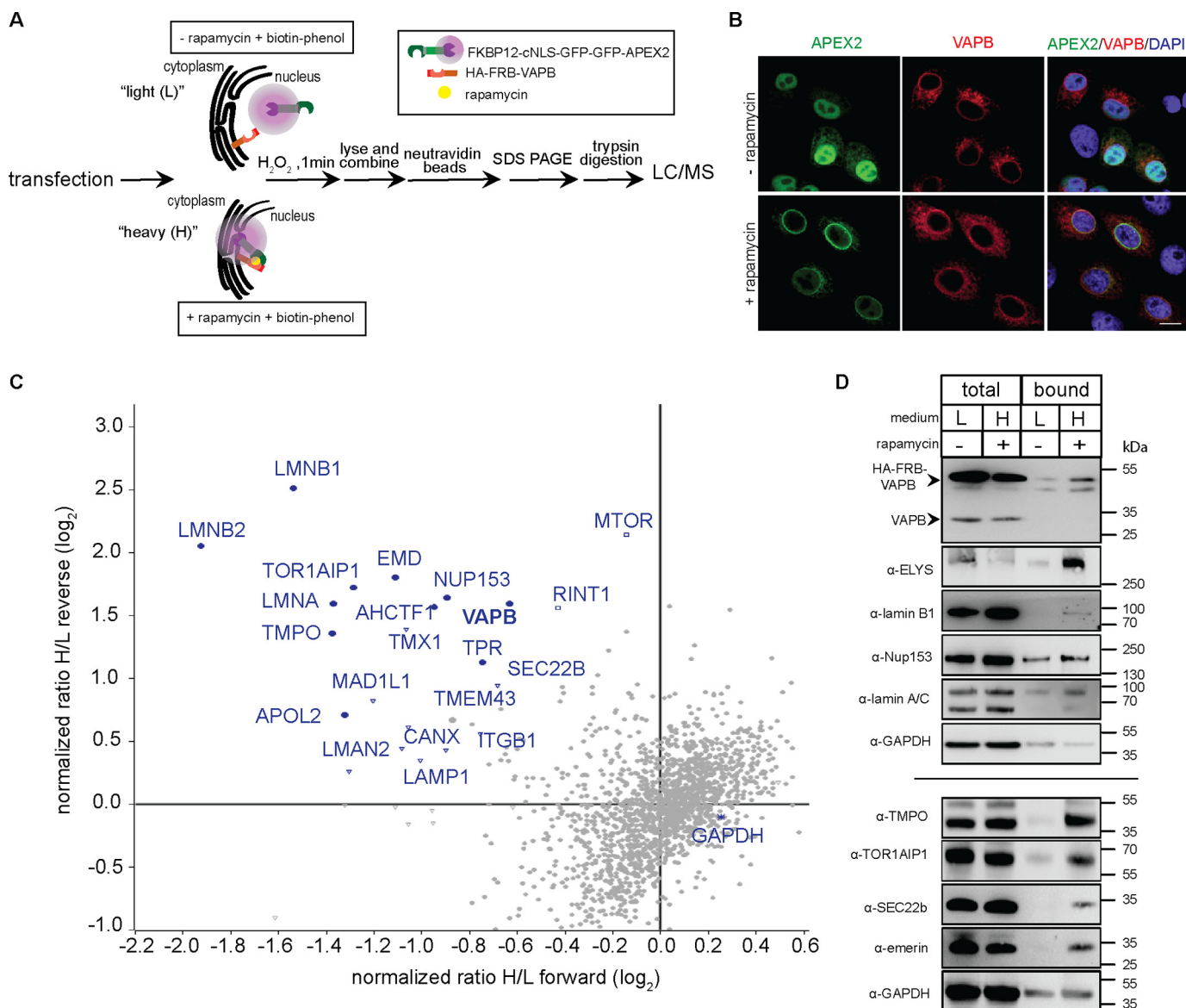


**Figure 4. RAPIDS using HA-FRB-VAPB.** *A*, experimental workflow. Cells are grown in light or heavy medium as indicated, cotransfected with plasmids coding for APEX2-dGFP-cNLS-FKBP12 and HA-FRB-VAPB, and subjected to RAPIDS as described in Fig. 3*A*. *B*, transfected cells were treated with or without rapamycin as indicated, fixed, and analyzed by fluorescence microscopy. Scale bar, 10  $\mu$ m. *C*, the scatter plot resulting from two independent experiments shows normalized  $\log_2$  ratios of proteins eluted from neutravidin beads in forward (heavy medium (H), without rapamycin; light (L) medium, with rapamycin; x axis) and reverse (heavy medium, with rapamycin; light medium, without rapamycin; y axis) experiments. As in Fig. 3, the plot focuses on the upper left quadrant. Closed circles, proteins that were significant in all experiments; open triangles, proteins that were significant only in forward experiments; open squares, proteins that were significant only in reverse experiments. *D*, total cell lysates (total) and proteins bound to neutravidin beads (bound) from experiments depicted in C were analyzed by Western blotting using antibodies against VAPB, ELYS, lamin B1, Nup153, lamin A/C, TMPO, TOR1AIP1, SEC22b, emerlin, and GAPDH as a loading control.

some extent (Fig. 1*C*), the efficiency of diffusion of proteins from the ER via the outer nuclear membrane to the INM in general is clearly affected by the size of the cytoplasmic domain (43–47). We therefore modified our approach 2-fold (Fig. 4*A*). First, we used a version of APEX2, APEX2-dGFP-NLS-FKBP12, that strongly accumulates in the nucleus of transfected cells as a result of its nuclear localization signal. Hence, biotinylation of nuclear proteins or INM proteins should be favored. Second, we designed a smaller version of VAPB, HA-FRB-VAPB, that we expected to diffuse more readily across the nuclear pore to the INM than the mCherry-tagged version. As shown in Fig. 4*B*, APEX2-dGFP-NLS-FKBP12 localized largely in the nucleus in the absence of rapamycin. Upon addition of

the drug, the reporter protein was sequestered to the nuclear envelope, suggesting binding to HA-FRB-VAPB at the INM. We then performed RAPIDS and could show that VAPB (*i.e.* HA-FRB-VAPB in this experiment) was prominently biotinylated in the presence of rapamycin (Fig. 4, *C* and *D*). By quantitative proteomics, we identified at least 22 biotinylated proteins that were enriched on the neutravidin beads upon addition of rapamycin to the cells, suggesting their close proximity to HA-FRB-VAPB (Fig. 4*C* and Table S2). Strikingly, many of the proteins identified are known to reside on the nuclear side of the nuclear envelope. The proximity candidates fall into three categories. In the first category are proteins of the INM like emerlin, lamina-associated polypeptide 1 (LAP1 or Torsin-1A–

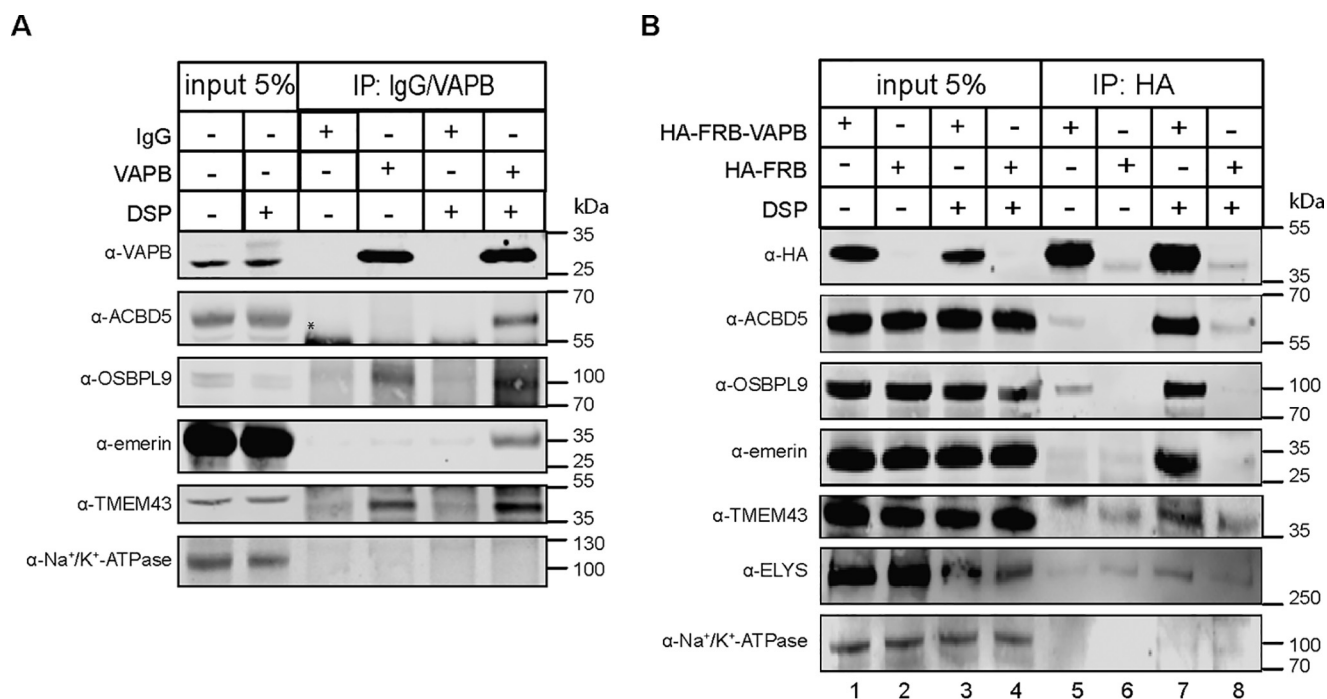


**Figure 5. VAPB forms complexes with emerlin, TMEM43, and ELYS.** A, HeLa cells were treated with (+) or without (-; DMSO as a control) DSP, and endogenous proteins from cell lysates were precipitated using rabbit anti-VAPB and rabbit IgG as a control. \*, IgG heavy chain. B, HeLa cells were transfected with constructs coding for HA-FRB-VAPB or HA-FRB and subjected to cross-linking with (+) or without (-; DMSO as a control) DSP. Proteins from cell lysates were immunoprecipitated (IP) using anti-HA antibodies. Note that HA-FRB was expressed and precipitated to similar levels as HA-FRB-VAPB (data not shown). A and B, precipitated proteins were analyzed by Western blotting, detecting VAPB, ACBD5, OSBPL9, emerlin, TMEM43, ELYS, the HA tag, and, as a control, Na<sup>+</sup>/K<sup>+</sup>-ATPase as indicated.

interacting protein 1 (TOR1AIP1) (48)) and LAP2 $\beta$  (thymopoietin (TMPO) (48, 49)). Another protein in this category is TMEM43, which we also found with mCherry-FRB-VAPB as a bait (Fig. 3). In the second category are proteins of the nuclear pore complex (NPC) like Nup153 (50), Tpr (51), and ELYS (AHCTF1 (52)). In the third category are components of the nuclear lamina like lamin A and lamin B (53). To confirm preferential biotinylation of candidates in the presence of rapamycin, we performed Western blotting of proteins eluted from the neutravidin beads (Fig. 4D). Essentially all the tested proteins showed increased recovery from neutravidin beads upon treatment of cells with rapamycin, including ELYS, lamin A/C, LAP1 (TOR1AIP1), LAP2 $\beta$  (TMPO), and emerlin. Together, our results show that RAPIDS allows the identification of known interaction partners of VAPB and, possibly, of novel proximity and/or interaction partners.

### Validation

Proteins identified by RAPIDS could be direct or indirect binding partners of VAPB and occur in biochemically stable complexes or just reside in very close proximity to our protein of interest. As a first step to distinguish between these possibilities, we performed coimmunoprecipitation experiments combined with a cross-linking approach to stabilize low-affinity interactions. We first immunoprecipitated endogenous VAPB using a specific antibody and analyzed the precipitate for coprecipitating proteins. As a control, total IgG was used (Fig. 5A). For the established binding partners of VAPB, ACBD5 and OSBPL9, and for emerlin and TMEM43, specific coprecipitation with VAPB was observed when the cells had been treated

with the cleavable bifunctional cross-linker dithiobis(succinimidyl propionate) (DSP). For OSBPL9 and TMEM43, coprecipitation above the IgG background was also seen in the absence of the cross-linker, suggesting tight interactions. To corroborate these findings, we also used HA-FRB-VAPB-overexpressing cells for coimmunoprecipitation experiments, again with and without DSP as a cross-linking reagent. As shown in Fig. 5B, low levels of ACBD5 and OSBPL9 coprecipitated with overexpressed HA-FRB-VAPB. The levels of coprecipitated proteins strongly increased when the cells had been treated with DSP prior to cell lysis (compare lanes 5 and 7). For emerlin, TMEM43, and to some extent ELYS, coprecipitation was observed in the cross-linked samples, suggesting that the corresponding complexes exist in intact cells. Very low levels of coprecipitating proteins were observed when the cells had been transfected with a plasmid coding for HA-FRB (lanes 6 and 8). Together, these results show that VAPB indeed interacts with some of the proteins that were identified as proximity partners by RAPIDS. It remains to be investigated whether these interactions are direct or indirect.

Next, we performed proximity ligation assays (PLAs) (54), which detect interactions (or at least proximity) of endogenous proteins and allow statements about the precise localization of the protein-protein interactions. These assays are based on the decoration of proteins in fixed cells, first with specific primary antibodies and subsequently with oligonucleotide-linked secondary antibodies. If the proteins of interest are in close proximity (*i.e.* within ~40 nm), subsequent ligation and amplification reactions lead to formation of a fluorescent product that

## Binding partners of VAPB at the inner nuclear membrane

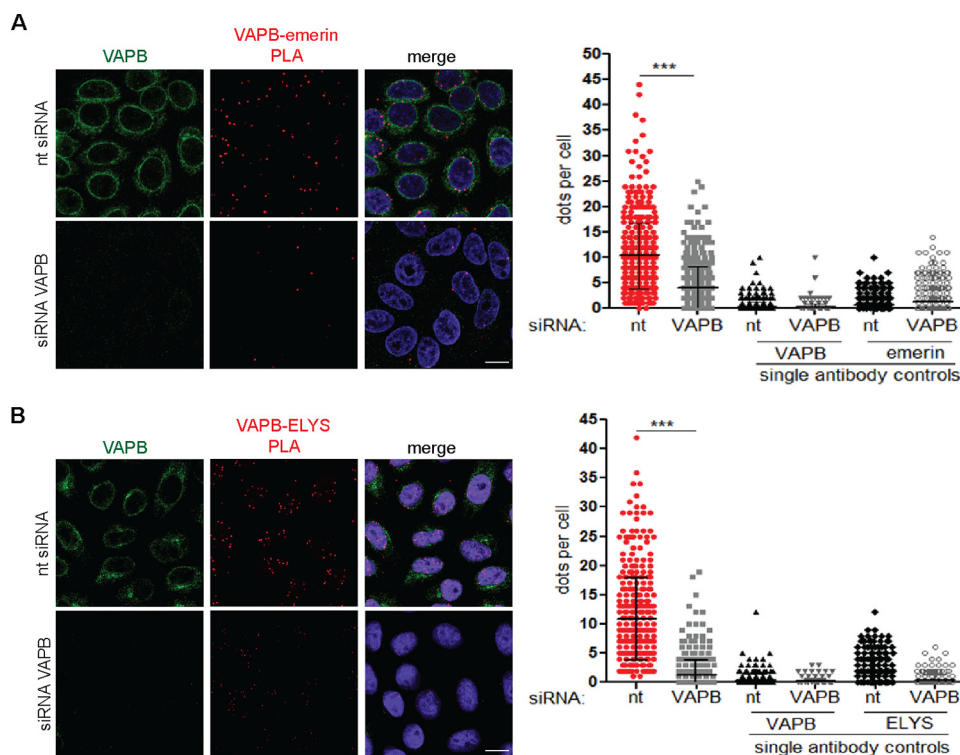


**Figure 6. VAPB is in close proximity to emerin and ELYS.** *A* and *B*, cells were treated with siRNAs against VAPB or nontargeting (*nt*) siRNAs as indicated and subjected to PLAs using antibodies against VAPB (*A* and *B*) and emerin (*A*) or ELYS (*B*), respectively. Indirect immunofluorescence was used to detect VAPB. The graphs show the quantification of PLA results from three independent experiments analyzing a total of 450 cells. The error bars indicate mean values  $\pm$  S.D. Single-antibody controls were performed to confirm the specificity of PLA interactions. \*\*\*,  $p < 0.001$ . Scale bars, 10  $\mu$ m.

can easily be detected by microscopy. We first analyzed VAPB with respect to its interaction with known binding partners that were also detected by RAPIDS, namely ACBD5 and OSBPL9. To characterize our antibodies, we performed immunofluorescence analysis. As shown in Fig. S3, *A* and *B*, ACBD5 colocalized with the peroxisomal marker protein PMP70, and OSBPL9 colocalized with the Golgi marker GM130, indicating the specificity of the ACBD5 and OSBPL9 antibodies. In PLAs, specific interactions of VAPB were observed with characteristic patterns of dots. For ACBD5 (Fig. S3, *C* and *D*), dots were found scattered all over the cell, consistent with signals derived from ER-peroxisome interactions. For OSBPL9, the observed dots were largely found in an area corresponding to the Golgi compartment (Fig. S3, *E* and *F*). The specificity of the signals was supported by single-antibody controls. These results show that our antibodies are suitable for a faithful detection of VAPB-protein interactions. Next, we performed PLAs with antibodies against VAPB and emerin or ELYS (Fig. 6). TMEM43 was not analyzed here due to lack of PLA-suitable antibodies. For emerin, PLA dots were mostly observed at the nuclear rim, consistent with the major localization of emerin at the INM (Fig. 6A). For ELYS (Fig. 6B), PLA dots were observed at the nuclear envelope but also in the nuclear interior. For both proteins, the number of dots decreased significantly when VAPB had been depleted by specific siRNAs as well as in single-antibody controls, demonstrating the specificity of the PLA. In summary, coimmunoprecipitation experiments and PLAs suggest that VAPB indeed forms complexes with proteins of the INM and/or the NPC. Fig. 7 depicts the interactome of VAPB, as revealed by our analysis and by previous studies.

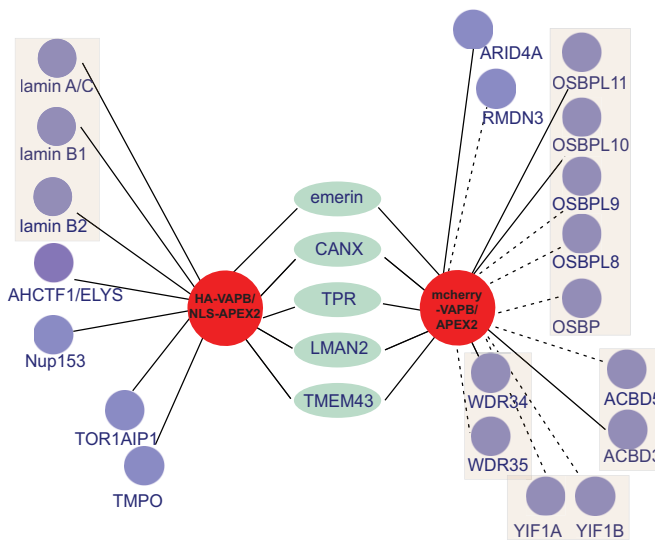


**Figure 7. The VAPB interactome.** Shown is a schematic representation of the protein network identified by RAPIDS using HA-FRB-VAPB (*HA-VAPB*) with APEX2-dGFP-cNLS-FKBP12 (*NLS-APEX2*) or mCherry-FRB-VAPB (*mCherry-VAPB*) with FKBP12-GFP-APEX2 (*APEX2*). Dotted lines indicate interactions that have also been found in previous studies.

## Discussion

### RAPIDS

The known binding partners of VAPB localize exclusively to the cytoplasm or to cytoplasmic membranes. The INM localization of VAPB therefore prompted us to search for nuclear proteins that could interact with VAPB or are at least in close proximity to VAPB at the level of the INM or the NPC. For this,



affinity-based methods that require an initial cell lysis step were not very promising because the lysis buffers must fulfill two conflicting criteria: they must be strong enough to solubilize protein complexes like the nuclear lamina or the NPC but maintain the interactions of interest. Indeed, validation of our candidate proteins by coimmunoprecipitation approaches required a careful choice of specific reaction conditions concerning the lysis buffer, the specific antibody, and, importantly, the cross-linker used for stabilization of protein–protein interactions. As alternatives, proximity-based approaches like BioID and the APEX system have the advantage of targeting proteins in their natural environment, living cells. BioID, in fact, was initially developed to probe the nuclear lamina for interaction partners of lamin A (18). In the last couple of years, APEX-based biotinylation approaches have been used very successfully for the analysis of the interactome of many proteins (9, 20–23, 25, 31–35). With RAPIDS, we now introduce a method that combines APEX2-dependent biotinylation, rapamycin-dependent targeting of the enzyme to proteins of interest, and quantitative proteomics using SILAC. The use of rapamycin to induce rapid targeting of APEX2 to a specific subcellular localization should facilitate the discrimination between proteins that are modified in a specific *versus* a nonspecific manner. Furthermore, a careful choice of the tags used for APEX2 (here,  $\pm$ NLS) and the protein of interest (here, HA *versus* mCherry) may strongly affect the spectrum of identified proteins. This is of particular importance for proteins of the INM, where the size and the nature of the tag may affect efficient targeting of proteins to their final destination. In general, the approach to physically separate the APEX2 enzyme from the protein of interest offers a tight control over the cellular proteins that are potential targets for biotinylation. This is a clear advantage for proteins like VAPB that can engage in interactions at different intracellular contact sites. Notably, a similar targeting approach using the rapamycin analogue AP21967 as a dimerizing agent was very recently described (55). In 2C-BioID, the authors used the rapamycin analogue AP21967 to initiate dimerization of a biotin-protein ligase and a protein of interest to analyze the interactomes of LAP2 $\beta$  and lamins A and C as a proof of principle.

The feasibility of RAPIDS was demonstrated by the identification of many of the previously known binding partners of VAPB (Fig. 3). Furthermore, we identified several novel nuclear proximity partners of VAPB, consistent with the INM localization of the protein. For this, usage of our nuclear version of APEX2 was important as it favors the biotinylation of nuclear proteins. Fig. 7 summarizes our findings and also indicates some of the proteins that had previously been identified as binding partners of VAPB. Altogether, RAPIDS is a versatile method for the identification of proteins that are in close proximity to a protein of interest. This modification of the classic APEX approach should be applicable to proteins residing at different subcellular localizations.

#### VAPB at the INM

To our knowledge, a nuclear localization of VAPB itself has not been documented so far, except in a very recent publication (30). Using our rapamycin-dependent dimerization assay as well as immunoelectron microscopy, we now unequivocally

show that VAPB can indeed reach the INM and can also be detected in close proximity to NPCs (Fig. 1). At this point, we cannot say with certainty which percentage of the entire cellular pool of endogenous VAPB resides at the INM. In immunofluorescence, the ratio of the nuclear envelope and the ER signals of VAPB is affected by the buffer conditions (Fig. 1A). In immunoelectron microscopy (Fig. 1D), epitope masking is a general issue and could affect nuclear and cytoplasmic immunoreactivity of VAPB differently. Hence, other, more quantitative methods are required for an accurate determination of VAPB levels at different localizations within the cell.

VAPB has been described as a protein that localizes to ER-contact sites (2). Using RAPIDS under conditions that should favor the identification of cytoplasmic binding/proximity partners (*i.e.* with mCherry-FRB-VAPB and FKBP12-GFP-APEX2; Figs. 2 and 3), we found many of the previously known interaction partners of VAPB, including oxysterol-binding proteins, PTPIP51, and ACBD5. Most of the identified proteins associate with membranes, and many of them localize to the ER (see Table S1), consistent with the major localization of mCherry-FRB-VAPB. Nevertheless, we also identified emerin as a mainly nuclear protein using this approach, in agreement with the observation that mCherry-FRB-VAPB can reach the INM (Fig. 1C). A different picture emerged when we used FRB-VAPB with an HA tag at the N-terminal end instead of an mCherry tag and APEX2-dGFP-NLS-FKBP12 as a nuclear version of the biotinylation enzyme (Fig. 4 and Table S2). Under this condition, we identified significantly more nuclear proteins, including emerin and other membrane proteins of the INM, several nucleoporins, and components of the nuclear lamina. This result is consistent with the observation that the efficiency of translocation of proteins from the outer to the inner nuclear membrane inversely correlates with the size of the cytoplasmic/nuclear region of the protein (43–47). Because the HA tag is significantly smaller than the mCherry tag, a larger proportion of the overexpressed protein is expected to reach the INM via passive diffusion (45) where, upon rapamycin treatment, the nuclear version of APEX2 can then initiate efficient biotinylation of neighboring proteins.

Importantly, interaction of endogenous VAPB or overexpressed VAPB with emerin and TMEM43 could be confirmed by coimmunoprecipitation experiments where the novel binding partners behaved very similarly to the established binding partners ACBD5 and OSBPL9 (Fig. 5). Interestingly, coprecipitation of TMEM43 with emerin has been described previously (36). For VAPB/emerin and VAPB/ELYS, we also confirmed a close proximity *in situ* using PLAs (Fig. 6). For emerin, PLA dots were largely restricted to the nuclear envelope, consistent with the predominant localization of the protein. ELYS is a nucleoporin that can also localize to the nuclear interior in interphase cells (52) and plays a role in early steps of postmitotic NPC assembly (56, 57). Hence, a role of VAPB in this process could be envisaged. ELYS has previously been suggested to interact directly with VAPB based on an FFAT-like motif in its sequence (2, 10). In our PLAs, we also observed intranuclear dots, suggesting that not only ELYS but also VAPB might reside in the nucleoplasm. This seems counterintuitive because VAPB is a membrane protein. Being a tail-anchored protein, however,

## Binding partners of VAPB at the inner nuclear membrane

a soluble pool of VAPB must exist, and a fraction could even reach the nuclear interior. At this point, we can only speculate about the functional significance of INM localization of VAPB. VAPB has been implicated in the transport of emerin and nucleoporins to the INM and the NPC, respectively (15).

In summary, our findings suggest that the interaction repertoire of VAPB is even larger than previously thought. VAPB not only serves as a bridging factor at multiple contact sites of the ER with mitochondria, peroxisomes, the Golgi apparatus, and the plasma membrane, but also localizes to the INM where it may contact several nucleoporins, integral membrane proteins, and components of the nuclear lamina.

### Experimental procedures

#### Plasmids

Standard procedures were used for cloning, and the obtained constructs were confirmed by sequencing. To obtain pcDNA3-FKBP12-GFP-APEX2, the FKBP12 coding sequence was originally derived from pcDNA3-FKBP12 (27, 58) using primers G1562 and G1563 and cloned into pcDNA3-Connexin43-GFP-APEX2 (Addgene plasmid 49385) through AflII and BamHI, thereby replacing the Connexin43 coding sequence (oligonucleotides are listed in Table S3). For APEX2-dGFP-NLS-FKBP12, the APEX2 coding sequence was amplified by PCR using pcDNA3-Connexin43-GFP-APEX2 as a template and primers G1573 and G1571. The PCR product was cloned into a pEGFP-C1 derivative encoding dGFP-cNLS-FKBP12 through BcuI. For pmCherry-FRB-VAPB, the VAPB coding sequence was amplified by PCR using primers G1390 and G1386 and pCAN-myc-VAPB (59) as a template. The PCR product was cloned into a pmCherry-C1 derivative coding for mCherry-FRB through KpnI and BamHI.

For pEF-HA-FRB-VAPB, the FRB coding sequence (as above) from mCherry-FRB was first inserted into a modified pEF-HA vector (60) via NcoI and EcoRI, generating pEF-HA-FRB. The VAPB coding sequence was amplified by PCR using primers G1512 and G1511 and pCAN-myc-VAPB (59) as a template. The PCR product was then inserted into pEF-HA-FRB plasmid through EcoRI and SpeI. To obtain pEGFP-APEX2, APEX2 was amplified from pcDNA3-FKBP12-GFP-APEX2 using primers G1854 and G1855 and cloned into pEGFP-C1 through EcoRI and BamHI. For APEX2-VAPB, VAPB was amplified from pmCherry-FRB-VAPB using primers G1512 and G1386 and cloned via EcoRI and BamHI into pAPEX2-C1, which had been generated by exchanging the mCherry sequence of pmCherry-C1 for that of APEX2.

#### Cell culture and transfection

HeLa P4 cells (61) were obtained from the National Institutes of Health AIDS Reagent Program. Cells were cultivated in Dulbecco's modified Eagle's medium (Life Technologies) supplemented with 10% (v/v) fetal bovine serum (Life Technologies), 100 units ml<sup>-1</sup> penicillin, 100 μg ml<sup>-1</sup> streptomycin, and 2 mM L-glutamine (Life Technologies) under 5% CO<sub>2</sub> at 37 °C. They were tested regularly for contamination by *Mycoplasma*.

For SILAC, cells were grown in medium containing heavy or light isotopes of arginine and lysine. For this purpose, Dulbecco's modified Eagle's medium (high glucose) lacking glutamine, lysine, and arginine (Thermo Fisher Scientific, Waltham, MA)

was supplemented with 10% (v/v) dialyzed fetal bovine serum, 6 mM L-glutamine (Life Technologies), 100 units ml<sup>-1</sup> penicillin, and 100 μg ml<sup>-1</sup> streptomycin. To obtain SILAC media with heavy and light isotopes, either 0.4 mM L-[<sup>13</sup>C<sub>6</sub>,<sup>15</sup>N<sub>2</sub>]lysine (Silantes, Munich, Germany) and 0.2 mM L-[<sup>13</sup>C<sub>6</sub>,<sup>15</sup>N<sub>4</sub>]arginine (Silantes) or 0.4 mM L-[<sup>12</sup>C<sub>6</sub>,<sup>14</sup>N<sub>2</sub>]lysine (Sigma-Aldrich) and 0.2 mM L-[<sup>12</sup>C<sub>6</sub>,<sup>14</sup>N<sub>4</sub>]arginine (Sigma-Aldrich) were added, respectively. To ensure sufficient incorporation of heavy amino acids, cells were passaged five to seven times in SILAC medium before the biotinylation experiment, and the incorporation rate was confirmed to be ≥97% by MS.

Transfections were performed according to the calcium phosphate method (62). Briefly, the respective plasmids were mixed with 250 mM CaCl<sub>2</sub>. After the addition of the same amount of HEPES buffer (50 mM HEPES, pH 6.98, 250 mM NaCl, and 1.5 mM NaHPO<sub>4</sub>) and 20-min incubation at room temperature, the mixture was added to the cells, which were then grown as above.

siRNA-mediated knockdown of VAPB was carried out using Lipofectamine RNAiMAX (Thermo Fisher Scientific) following the manufacturer's protocol. VAPB siRNA (GCUCUUGGCUCUGGUGGUUUU and AAAACCACCAGAGCCAAGAGC; Sigma) and ON-Targetplus nontargeting siRNA (D-001810-01-50, Dharmacon, Lafayette, CO) were used at a final concentration of 100 nM.

#### Rapamycin-dependent biotinylation assay

HeLa P4 cells were grown in 10-cm dishes in SILAC medium as described above. Two sets of cells (in light or heavy medium) were transfected with pmCherry-FRB-VAPB and pcDNA3-FKBP12-GFP-APEX2 or pEF-HA-FRB-VAPB and pAPEX2-dGFP-NLS-FKBP12, using the same transfection mixture to ensure similar expression levels, and grown to confluence. Cells were then incubated for 30 min with 500 μM biotin-phenol (Iris Biotech, Marktredwitz, Germany) with or without 200 nM rapamycin (Sigma-Aldrich). For each experiment, forward and reverse reactions were performed. For forward reactions, cells grown in light SILAC medium were treated with rapamycin, and cells grown in heavy SILAC medium were not. For reverse reactions, this labeling scheme was switched. After incubation with biotin-phenol and rapamycin, 1 mM H<sub>2</sub>O<sub>2</sub> was added at room temperature. After 1 min, the medium was aspirated, and cells were washed twice with quenching buffer (5 mM Trolox, 10 mM NaN<sub>3</sub>, and 10 mM sodium ascorbate in PBS) and once with PBS. Cells used for fluorescence microscopy were fixed immediately.

For Western blotting and SILAC analyses, cells from each dish were lysed with 1 ml of radioimmune precipitation assay buffer (50 mM Tris, pH 7.4, 5 mM Trolox, 0.5% (w/v) sodium deoxycholate, 150 mM NaCl, 0.1% (w/v) sodium dodecyl sulfate (SDS), 1% (v/v) Triton X-100, 1 mM phenylmethanesulfonyl fluoride, 10 mM NaN<sub>3</sub>, 10 mM sodium ascorbate, 1 μg ml<sup>-1</sup> aprotinin, 1 μg ml<sup>-1</sup> leupeptin, and 1 μg ml<sup>-1</sup> pepstatin). The cell lysate was incubated for 5 min on ice and centrifuged for 10 min at 16,000 × g at 4 °C. The cleared cell lysate was used to enrich biotinylated proteins with neutravidin beads (Thermo Fisher Scientific). For MS, cell lysates derived from three 10-cm dishes were pooled, the protein concentration of the cell lysates

was determined using the Pierce 660 nm Protein Assay (Thermo Fisher Scientific), and equal protein amounts of samples treated with or without rapamycin were mixed prior to addition to neutravidin beads. For Western blotting analyses, the samples were kept separately. For each forward or reverse experiment, six batches of 130  $\mu$ l of neutravidin beads were incubated with 1 ml of cell lysate overnight at 4 °C on a rotor. The beads were washed once with washing buffer 1 (50 mM HEPES, pH 7.4, 0.1% (w/v) sodium deoxycholate, 1% (v/v) Triton X-100, 500 mM NaCl, and 1 mM EDTA), once with washing buffer 2 (50 mM Tris, pH 8.0, 250 mM LiCl, 0.5% (v/v) Nonidet P-40, 0.5% (w/v) sodium deoxycholate, and 1 mM EDTA), and twice with washing buffer 3 (50 mM Tris, pH 7.4, and 50 mM NaCl). For each washing step, the beads were incubated for 8 min at 4 °C on a rotor. After the last washing step, the buffer was removed, and bound proteins were eluted from the beads by incubation for 5 min at 95 °C with 90  $\mu$ l of SDS sample buffer (4% (w/v) SDS, 125 mM Tris, pH 6.8, 10% (v/v) glycerol, 0.02% (v/v) bromophenol blue, and 10% (v/v)  $\beta$ -mercaptoethanol) supplemented with 5 mM desthiobiotin (Sigma-Aldrich). To increase the protein concentration, three batches of beads were consecutively eluted in the same buffer.

### Mass spectrometric analyses

Samples were separated on 4–12% NuPAGE Novex Bis-Tris minigels (Invitrogen). Gels were stained with Coomassie Blue, and each lane was sliced into 11–12 equidistant bands. After washing, gel slices were reduced with dithiothreitol (DTT), alkylated with 2-iodoacetamide, and digested with trypsin (sequencing grade; Promega, Madison, WI) overnight. The resulting peptide mixtures were then extracted, dried in a SpeedVac, reconstituted in 2% acetonitrile and 0.1% formic acid (v/v), and analyzed by nano-LC-MS/MS on a hybrid quadrupole/orbitrap mass spectrometer (Q Exactive, Thermo Fisher Scientific) as described previously (63). Raw data were processed using MaxQuant software version 1.5.7.4 (Max Planck Institute for Biochemistry, Martinsried, Germany). Proteins were identified against the human reference proteome (v2017.02, 92,927 protein entries) along with a set of common lab contaminants. The search was performed with trypsin (excluding proline-proximal cleavage sites) as enzyme and iodoacetamide as cysteine blocking agent. Up to two missed tryptic cleavages were allowed as well as methionine oxidation and protein N-terminal acetylation variable modifications. Instrument type “Orbitrap” was selected to adjust for MS acquisition specifics. Following an initial internal recalibration, this translated into an MS mass tolerance of 4.5 ppm and an MS/MS mass tolerance of 20 ppm. Protein and peptide results lists were thresholded at false discovery rates of 0.01 using a forward-and-reverse decoy database approach. The arginine R10 and lysine K8 labels including the “Re-quantify” option were specified for relative protein quantitation. Perseus software version 1.5.6.0 (Max Planck Institute for Biochemistry, Martinsried, Germany) was used for statistical evaluation of relative protein quantitation values from the MaxQuant software results, and a two-sided significance B test (64) was performed using normalized  $\log_2$  ratios. For the analysis, a Benjamini–Hochberg correction was applied, and a threshold value of 0.05 was chosen. Mass

spectrometry experiments were performed twice, each with two biological and two technical replicates.

### Data availability

The MS proteomics data have been deposited to the ProteomeXchange Consortium via the PRIDE (65) partner repository with the data set identifier PXD012157.

### Western blotting analyses

Western blotting was performed according to standard methods using HRP-coupled secondary antibodies. To detect biotinylated proteins, they were separated by SDS-PAGE using 4–12% NuPAGE Novex Bis-Tris minigels. After transfer to nitrocellulose, the membranes were incubated in blocking buffer (3% bovine serum albumin (BSA) in TBS-T (24.8 mM Tris, pH 7.4, 137 mM NaCl, 2.7 mM KCl, and 1% (v/v) Tween 20)) overnight at 4 °C. Incubation with streptavidin-HRP (Jackson ImmunoResearch Laboratories, West Grove, PA; diluted 1:5,000–1:40,000 in blocking buffer) for 1 h at room temperature was followed by three washing steps with TBS-T. For detection of proteins, Immobilon Western Chemiluminescent HRP Substrate (Millipore, Burlington, MA) and a luminescence image analyzer (LAS-3000, Fuji, Tokyo, Japan) were used. Signal intensities were measured using Image Studio Lite (version 5.2). Two-way analysis of variance followed by Bonferroni post-test was used for statistical analysis, and a confidence interval of 95% was set. Primary and secondary antibodies are listed in Table S4.

### Immunofluorescence and microscopy

For fluorescence microscopy, cells were grown on coverslips and fixed with 4% (v/v) paraformaldehyde. Cells expressing fluorescently labeled proteins were mounted directly with Mowiol supplemented with 1  $\mu$ g/ml DAPI. For immunofluorescence, fixed cells were permeabilized with 0.5% (v/v) Triton X-100 in PBS for 5 min at room temperature and blocked with 3% (w/v) BSA in PBS for 20 min at room temperature. Staining was performed for 1 h at room temperature using appropriate primary antibodies and fluorescently labeled secondary antibodies (Table S4), which were diluted in 3% BSA in PBS. Afterwards, cells were embedded in Mowiol–DAPI. Microscopic analysis was performed using an LSM510 confocal laser-scanning microscope using a 63 $\times$ /1.4 oil immersion lens (Zeiss, Oberkochen, Germany).

### EM

For immunoelectron microscopy, HeLa cells were fixed with 2% paraformaldehyde and 0.2% glutaraldehyde in PHEM buffer (60 mM Pipes, 25 mM HEPES, 2 mM MgCl<sub>2</sub>, and 10 mM EGTA, pH 6.9) for 1 h, washed with PHEM buffer, and scraped off. Cells were pelleted (200  $\times$  g for 2 min), resuspended in 0.1% glycine in PBS, pelleted (400  $\times$  g for 2 min), resuspended in 0.1% glycine in PBS (15 min), pelleted (400  $\times$  g for 2 min), resuspended in 1% gelatin (Dr. Oetker) at 37 °C for 10 min, pelleted (400  $\times$  g for 2 min), resuspended in 10% gelatin for 10 min at 37 °C, and then replaced on ice. Pellets were immersed in 15% polyvinylpyrrolidone (10 kDa; Sigma) and 1.7 M sucrose in PBS overnight, then mounted and frozen in liquid nitrogen, and

## Binding partners of VAPB at the inner nuclear membrane

sectioned on a cryo-ultramicrotome (Leica UC6 with FC6). Cryosections were thawed and placed at 37 °C, washed in 0.1% BSA (Sigma) in PBS and then in 1% BSA in PBS for 3 min followed by overnight incubation with undiluted primary antibody (mouse anti-VAPB mouse, Proteintech), washed in PBS, incubated with 10-nm colloidal gold–anti-mouse antibody (BBI Solutions). Grids were washed in PBS, transferred to 1% glutaraldehyde in PBS (5 min), washed in H<sub>2</sub>O, and embedded in 2% methyl cellulose containing 0.4% uranyl acetate (Agar Scientific). Imaging was done using a Hitachi H7600 transmission electron microscope at 100 kV.

### Cross-linking and coimmunoprecipitation

2 × 10<sup>6</sup> HeLa P4 cells/10-cm dish were transfected with plasmids coding for HA-FRB-VAPB or HA-FRB. After 24 h, the cells were washed twice with cold PBS containing 0.1 mM CaCl<sub>2</sub> and 1 mM MgCl<sub>2</sub> and incubated with DSP (Thermo Scientific) at a final concentration of 1 mM in DMSO for 2 h on ice. For control reactions, DMSO alone was used. DSP was quenched by the addition of 20 mM Tris-HCl, pH 7.4, for 15 min. The cells were then washed twice with cold PBS and lysed with 1 ml of lysis buffer (0.5% sodium deoxycholate, 50 mM Tris-HCl, pH 7.4, 150 mM NaCl, 0.25% SDS, and 0.5% Triton X-100 with Complete protease inhibitor mixture (Roche Applied Science)) for 30 min on ice. To reduce viscosity, the lysate was passed through a 27-gauge × 3/4-inch needle and then centrifuged at 15,000 × *g* for 20 min at 4 °C. For immunoprecipitation, 25 μl of anti-HA–agarose beads (Sigma A2095) were washed with washing buffer (10 mM HEPES, 150 mM NaCl, 1 mM EGTA, 0.1 mM MgCl<sub>2</sub>, 0.1% Triton X-100, and Complete protease inhibitor mixture). The lysate from 24 × 10<sup>6</sup> cells was added to the beads and rotated for 3 h at 4 °C. The beads were then washed four times with washing buffer, and proteins were eluted with sample buffer containing 50 mM DTT. For immunoprecipitation of endogenous protein complexes, 4 μg of rabbit anti-VAPB, or IgG as a control were immobilized on 40 μl of Protein A–Sepharose 4 Fast Flow beads (GE Healthcare) for 3 h and incubated with lysates from 24 × 10<sup>6</sup> cells that had or had not been subjected to cross-linking as described above.

### PLA

HeLa cells were seeded at a density of 40,000 cells/well in 24-well plates. After 48 h, cells were fixed with 4% paraformaldehyde and permeabilized with 0.05% (v/v) Triton X-100. PLAs were performed using the Duolink *In Situ* PLA kit (DUO 9200, Sigma-Aldrich). Cells were blocked and incubated with mouse anti-VAPB and rabbit anti-emerin, rabbit anti-ELYS, rabbit anti-ACBD5, or rabbit anti-OSBPL9, respectively (see Table S4 for antibodies). After ligation and amplification using the corresponding PLA probes, the cells were counterstained for VAPB and mounted using Duolink mounting medium with DAPI. Images were acquired on an LSM510 confocal laser-scanning microscope using a 63×/1.4 oil immersion lens. 450 cells over three independent experiments were analyzed for PLA interaction using CellProfiler 2.2 (66). One-way analysis of variance followed by Bonferroni post-test was used for statistical analysis, and a confidence interval of 95% was set.

**Author contributions**—C. J., M. M., M. W. G., and C. L. data curation; C. J., M. M., M. W. G., C. L., H. U., and R. H. K. formal analysis; C. J., M. M., and M. W. G. investigation; C. J., M. M., M. W. G., C. L., and H. U. methodology; C. J., M. M., C. L., H. U., and R. H. K. writing-review and editing; C. L., H. U., and R. H. K. supervision; C. L., H. U., and R. H. K. project administration; H. U. and R. H. K. funding acquisition; R. H. K. conceptualization; R. H. K. writing-original draft.

**Acknowledgments**—We thank Thierry Wasselin and Christiane Spillner (University Medical Center Göttingen, Germany) and Christine Richardson (School of Biological and Biomedical Sciences, Durham University, UK) for expert technical assistance; Drs. Eric Schirmer (Edinburgh, Scotland), Nica Borgese (Milan, Italy), and Sima Lev (Rehovot, Israel) for valuable reagents; and Dr. Eric Arakel (Göttingen) for advice.

### References

1. Lev, S., Ben Halevy, D., Peretti, D., and Dahan, N. (2008) The VAP protein family: from cellular functions to motor neuron disease. *Trends Cell Biol.* **18**, 282–290 [CrossRef Medline](#)
2. Murphy, S. E., and Levine, T. P. (2016) VAP, a versatile access point for the endoplasmic reticulum: review and analysis of FFAT-like motifs in the VAPome. *Biochim. Biophys. Acta* **1861**, 952–961 [CrossRef Medline](#)
3. Casson, J., McKenna, M., Haßdenteufel, S., Aviram, N., Zimmerman, R., and High, S. (2017) Multiple pathways facilitate the biogenesis of mammalian tail-anchored proteins. *J. Cell Sci.* **130**, 3851–3861 [CrossRef Medline](#)
4. Kutay, U., Hartmann, E., and Rapoport, T. A. (1993) A class of membrane proteins with a C-terminal anchor. *Trends Cell Biol.* **3**, 72–75 [CrossRef Medline](#)
5. Costello, J. L., Castro, I. G., Hacker, C., Schrader, T. A., Metz, J., Zeuschner, D., Azadi, A. S., Godinho, L. F., Costina, V., Findeisen, P., Manner, A., Islinger, M., and Schrader, M. (2017) ACBD5 and VAPB mediate membrane associations between peroxisomes and the ER. *J. Cell Biol.* **216**, 331–342 [CrossRef Medline](#)
6. Stoica, R., De Vos, K. J., Paillusson, S., Mueller, S., Sancho, R. M., Lau, K. F., Vizcay-Barrera, G., Lin, W. L., Xu, Y. F., Lewis, J., Dickson, D. W., Petrucelli, L., Mitchell, J. C., Shaw, C. E., and Miller, C. C. (2014) ER-mitochondria associations are regulated by the VAPB-PTPIP51 interaction and are disrupted by ALS/FTD-associated TDP-43. *Nat. Commun.* **5**, 3996 [CrossRef Medline](#)
7. Kuijpers, M., Yu, K. L., Teuling, E., Akhmanova, A., Jaarsma, D., and Hoogenraad, C. C. (2013) The ALS8 protein VAPB interacts with the ER-Golgi recycling protein YIF1A and regulates membrane delivery into dendrites. *EMBO J.* **32**, 2056–2072 [CrossRef Medline](#)
8. Moustaqim-Barrette, A., Lin, Y. Q., Pradhan, S., Neely, G. G., Bellen, H. J., and Tsuda, H. (2014) The amyotrophic lateral sclerosis 8 protein, VAP, is required for ER protein quality control. *Hum. Mol. Genet.* **23**, 1975–1989 [CrossRef Medline](#)
9. Johnson, B., Leek, A. N., Solé, L., Maverick, E. E., Levine, T. P., and Tamkun, M. M. (2018) Kv2 potassium channels form endoplasmic reticulum/plasma membrane junctions via interaction with VAPA and VAPB. *Proc. Natl. Acad. Sci. U.S.A.* **115**, E7331–E7340 [CrossRef Medline](#)
10. Huttlin, E. L., Ting, L., Bruckner, R. J., Gebreab, F., Gygi, M. P., Szpyt, J., Tam, S., Zarraga, G., Colby, G., Baltier, K., Dong, R., Guarani, V., Vaites, L. P., Ordureau, A., Rad, R., et al. (2015) The BioPlex Network: a systematic exploration of the human interactome. *Cell* **162**, 425–440 [CrossRef Medline](#)
11. Murphy, R., and Wenthe, S. R. (1996) An RNA-export mediator with an essential nuclear export signal. *Nature* **383**, 357–360 [CrossRef Medline](#)
12. Loewen, C. J., Roy, A., and Levine, T. P. (2003) A conserved ER targeting motif in three families of lipid binding proteins and in Opi1p binds VAP. *EMBO J.* **22**, 2025–2035 [CrossRef Medline](#)

13. Baron, Y., Pedrioli, P. G., Tyagi, K., Johnson, C., Wood, N. T., Fontaine, D., Wightman, M., and Alexandru, G. (2014) VAPB/ALS8 interacts with FFAT-like proteins including the p97 cofactor FAF1 and the ASNA1 AT-Pase. *BMC Biol.* **12**, 39 [CrossRef Medline](#)
14. Nishimura, A. L., Mitne-Neto, M., Silva, H. C., Richieri-Costa, A., Middleton, S., Cascio, D., Kok, F., Oliveira, J. R., Gillingwater, T., Webb, J., Skehel, P., and Zatz, M. (2004) A mutation in the vesicle-trafficking protein VAPB causes late-onset spinal muscular atrophy and amyotrophic lateral sclerosis. *Am. J. Hum. Genet.* **75**, 822–831 [CrossRef Medline](#)
15. Tran, D., Chalhoub, A., Schooley, A., Zhang, W., and Ngsee, J. K. (2012) A mutation in VAPB that causes amyotrophic lateral sclerosis also causes a nuclear envelope defect. *J. Cell Sci.* **125**, 2831–2836 [CrossRef Medline](#)
16. Gingras, A. C., Abe, K. T., and Raught, B. (2019) Getting to know the neighborhood: using proximity-dependent biotinylation to characterize protein complexes and map organelles. *Curr. Opin. Chem. Biol.* **48**, 44–54 [CrossRef Medline](#)
17. Kim, D. I., and Roux, K. J. (2016) Filling the void: proximity-based labeling of proteins in living cells. *Trends Cell Biol.* **26**, 804–817 [CrossRef Medline](#)
18. Roux, K. J., Kim, D. I., Raida, M., and Burke, B. (2012) A promiscuous biotin ligase fusion protein identifies proximal and interacting proteins in mammalian cells. *J. Cell Biol.* **196**, 801–810 [CrossRef Medline](#)
19. Branon, T. C., Bosch, J. A., Sanchez, A. D., Udeshi, N. D., Svinkina, T., Carr, S. A., Feldman, J. L., Perrimon, N., and Ting, A. Y. (2018) Efficient proximity labeling in living cells and organisms with TurboID. *Nat. Biotechnol.* **36**, 880–887 [CrossRef Medline](#)
20. Rhee, H. W., Zou, P., Udeshi, N. D., Martell, J. D., Mootha, V. K., Carr, S. A., and Ting, A. Y. (2013) Proteomic mapping of mitochondria in living cells via spatially restricted enzymatic tagging. *Science* **339**, 1328–1331 [CrossRef Medline](#)
21. Udeshi, N. D., Pedram, K., Svinkina, T., Fereshetian, S., Myers, S. A., Aygun, O., Clauser, K., Ryan, D., Ast, T., Mootha, V. K., Ting, A. Y., and Carr, S. A. (2017) Antibodies to biotin enable large-scale detection of biotinylation sites on proteins. *Nat. Methods* **14**, 1167–1170 [CrossRef Medline](#)
22. Lobingier, B. T., Hüttenhain, R., Eichel, K., Miller, K. B., Ting, A. Y., von Zastrow, M., and Krogan, N. J. (2017) An approach to spatiotemporally resolve protein interaction networks in living cells. *Cell* **169**, 350–360.e12 [CrossRef Medline](#)
23. Mick, D. U., Rodrigues, R. B., Leib, R. D., Adams, C. M., Chien, A. S., Gygi, S. P., and Nachury, M. V. (2015) Proteomics of primary cilia by proximity labeling. *Dev. Cell* **35**, 497–512 [CrossRef Medline](#)
24. Lam, S. S., Martell, J. D., Kamer, K. J., Deerinck, T. J., Ellisman, M. H., Mootha, V. K., and Ting, A. Y. (2015) Directed evolution of APEX2 for electron microscopy and proximity labeling. *Nat. Methods* **12**, 51–54 [CrossRef Medline](#)
25. Hung, V., Zou, P., Rhee, H. W., Udeshi, N. D., Cracan, V., Svinkina, T., Carr, S. A., Mootha, V. K., and Ting, A. Y. (2014) Proteomic mapping of the human mitochondrial intermembrane space in live cells via radiometric APEX tagging. *Mol. Cell* **55**, 332–341 [CrossRef Medline](#)
26. Bar, D. Z., Atkatsch, K., Tavarez, U., Erdos, M. R., Gruenbaum, Y., and Collins, F. S. (2018) Biotinylation by antibody recognition—a method for proximity labeling. *Nat. Methods* **15**, 127–133 [CrossRef Medline](#)
27. Pfaff, J., Rivera Monroy, J., Jamieson, C., Rajanala, K., Vilardi, F., Schwappach, B., and Kehlenbach, R. H. (2016) Emery-Dreifuss muscular dystrophy mutations impair TRC40-mediated targeting of emerin to the inner nuclear membrane. *J. Cell Sci.* **129**, 502–516 [CrossRef Medline](#)
28. Chen, J., Zheng, X. F., Brown, E. J., and Schreiber, S. L. (1995) Identification of an 11-kDa FKBP12-rapamycin-binding domain within the 289-kDa FKBP12-rapamycin-associated protein and characterization of a critical serine residue. *Proc. Natl. Acad. Sci. U.S.A.* **92**, 4947–4951 [CrossRef Medline](#)
29. Cheng, L. C., Baboo, S., Lindsay, C., Brusman, L., Martinez-Bartolomé, S., Tapia, O., Zhang, X., Yates, J. R., 3rd, and Gerace, L. (2019) Identification of new transmembrane proteins concentrated at the nuclear envelope using organellar proteomics of mesenchymal cells. *Nucleus* **10**, 126–143 [CrossRef Medline](#)
30. Saiz-Ros, N., Czapiewski, R., Epifano, I., Stevenson, A., Swanson, S. K., Dixon, C. R., Zamora, D. B., McElwee, M., Vijaykrishnan, S., Richardson, C. A., Dong, L., Kelly, D. A., Pytowski, L., Goldberg, M. W., Florens, L., et al. (2019) Host vesicle fusion protein VAPB contributes to the nuclear egress stage of herpes simplex virus type-1 (HSV-1) replication. *Cells* **8**, E120 [CrossRef Medline](#)
31. Cho, I. T., Adelmant, G., Lim, Y., Marto, J. A., Cho, G., and Golden, J. A. (2017) Ascorbate peroxidase proximity labeling coupled with biochemical fractionation identifies promoters of endoplasmic reticulum-mitochondrial contacts. *J. Biol. Chem.* **292**, 16382–16392 [CrossRef Medline](#)
32. Han, S., Udeshi, N. D., Deerinck, T. J., Svinkina, T., Ellisman, M. H., Carr, S. A., and Ting, A. Y. (2017) Proximity biotinylation as a method for mapping proteins associated with mtDNA in living cells. *Cell Chem. Biol.* **24**, 404–414 [CrossRef Medline](#)
33. Hung, V., Lam, S. S., Udeshi, N. D., Svinkina, T., Guzman, G., Mootha, V. K., Carr, S. A., and Ting, A. Y. (2017) Proteomic mapping of cytosol-facing outer mitochondrial and ER membranes in living human cells by proximity biotinylation. *Elife* **6**, e24463 [CrossRef Medline](#)
34. Lee, S. Y., Kang, M. G., Park, J. S., Lee, G., Ting, A. Y., and Rhee, H. W. (2016) APEX fingerprinting reveals the subcellular localization of proteins of interest. *Cell Rep.* **15**, 1837–1847 [CrossRef Medline](#)
35. Paek, J., Kalocsay, M., Staus, D. P., Winkler, L., Pascolutti, R., Paulo, J. A., Gygi, S. P., and Kruse, A. C. (2017) Multidimensional tracking of GPCR signaling via peroxidase-catalyzed proximity labeling. *Cell* **169**, 338–349.e11 [CrossRef Medline](#)
36. Bengtsson, L., and Otto, H. (2008) LUMA interacts with emerin and influences its distribution at the inner nuclear membrane. *J. Cell Sci.* **121**, 536–548 [CrossRef Medline](#)
37. Liang, W. C., Mitsuhashi, H., Keduka, E., Nonaka, I., Noguchi, S., Nishino, I., and Hayashi, Y. K. (2011) TMEM43 mutations in Emery-Dreifuss muscular dystrophy-related myopathy. *Ann. Neurol.* **69**, 1005–1013 [CrossRef Medline](#)
38. Franke, W. W., Dörflinger, Y., Kuhn, C., Zimbelmann, R., Winter-Simanowski, S., Frey, N., and Heid, H. (2014) Protein LUMA is a cytoplasmic plaque constituent of various epithelial adherens junctions and composite junctions of myocardial intercalated disks: a unifying finding for cell biology and cardiology. *Cell Tissue Res.* **357**, 159–172 [CrossRef Medline](#)
39. Defeo-Jones, D., Huang, P. S., Jones, R. E., Haskell, K. M., Vuocolo, G. A., Hanobik, M. G., Huber, H. E., and Oliff, A. (1991) Cloning of cDNAs for cellular proteins that bind to the retinoblastoma gene product. *Nature* **352**, 251–254 [CrossRef Medline](#)
40. Wu, M. Y., Eldin, K. W., and Beaudet, A. L. (2008) Identification of chromatin remodeling genes Arid4a and Arid4b as leukemia suppressor genes. *J. Natl. Cancer Inst.* **100**, 1247–1259 [CrossRef Medline](#)
41. Cartegni, L., di Barletta, M. R., Barresi, R., Squarzone, S., Sabatelli, P., Maraldi, N., Mora, M., Di Blasi, C., Cornelio, F., Merlini, L., Villa, A., Cobianchi, F., and Toniolo, D. (1997) Heart-specific localization of emerin: new insights into Emery-Dreifuss muscular dystrophy. *Hum. Mol. Genet.* **6**, 2257–2264 [CrossRef Medline](#)
42. Salpingidou, G., Smertenko, A., Hausmanowa-Petruciewicz, I., Hussey, P. J., and Hutchison, C. J. (2007) A novel role for the nuclear membrane protein emerin in association of the centrosome to the outer nuclear membrane. *J. Cell Biol.* **178**, 897–904 [CrossRef Medline](#)
43. Ohba, T., Schirmer, E. C., Nishimoto, T., and Gerace, L. (2004) Energy- and temperature-dependent transport of integral proteins to the inner nuclear membrane via the nuclear pore. *J. Cell Biol.* **167**, 1051–1062 [CrossRef Medline](#)
44. Soullam, B., and Worman, H. J. (1995) Signals and structural features involved in integral membrane protein targeting to the inner nuclear membrane. *J. Cell Biol.* **130**, 15–27 [CrossRef Medline](#)
45. Ungricht, R., Klann, M., Horvath, P., and Kutay, U. (2015) Diffusion and retention are major determinants of protein targeting to the inner nuclear membrane. *J. Cell Biol.* **209**, 687–703 [CrossRef Medline](#)
46. Zuleger, N., Kelly, D. A., Richardson, A. C., Kerr, A. R., Goldberg, M. W., Goryachev, A. B., and Schirmer, E. C. (2011) System analysis shows distinct mechanisms and common principles of nuclear envelope protein dynamics. *J. Cell Biol.* **193**, 109–123 [CrossRef Medline](#)
47. Blenski, M., and Kehlenbach, R. H. (2019) Targeting of LRRC59 to the endoplasmic reticulum and the inner nuclear membrane. *Int. J. Mol. Sci.* **20**, E334 [CrossRef Medline](#)

## Binding partners of VAPB at the inner nuclear membrane

48. Foisner, R., and Gerace, L. (1993) Integral membrane proteins of the nuclear envelope interact with lamins and chromosomes, and binding is modulated by mitotic phosphorylation. *Cell*. **73**, 1267–1279 [CrossRef](#) [Medline](#)
49. Furukawa, K., Panté, N., Aebi, U., and Gerace, L. (1995) Cloning of a cDNA for lamina-associated polypeptide 2 (LAP2) and identification of regions that specify targeting to the nuclear envelope. *EMBO J.* **14**, 1626–1636 [CrossRef](#) [Medline](#)
50. Sukegawa, J., and Blobel, G. (1993) A nuclear pore complex protein that contains zinc finger motifs, binds DNA, and faces the nucleoplasm. *Cell* **72**, 29–38 [CrossRef](#) [Medline](#)
51. Cordes, V. C., Reidenbach, S., Rackwitz, H. R., and Franke, W. W. (1997) Identification of protein p270/Tpr as a constitutive component of the nuclear pore complex-attached intranuclear filaments. *J. Cell Biol.* **136**, 515–529 [CrossRef](#) [Medline](#)
52. Rasala, B. A., Orjalo, A. V., Shen, Z., Briggs, S., and Forbes, D. J. (2006) ELYS is a dual nucleoporin/kinetochore protein required for nuclear pore assembly and proper cell division. *Proc. Natl. Acad. Sci. U.S.A.* **103**, 17801–17806 [CrossRef](#) [Medline](#)
53. Gerace, L., and Blobel, G. (1980) The nuclear envelope lamina is reversibly depolymerized during mitosis. *Cell* **19**, 277–287 [CrossRef](#) [Medline](#)
54. Söderberg, O., Gullberg, M., Jarvius, M., Ridderstråle, K., Leuchowius, K. J., Jarvius, J., Wester, K., Hydbring, P., Bahram, F., Larsson, L. G., and Landegren, U. (2006) Direct observation of individual endogenous protein complexes in situ by proximity ligation. *Nat. Methods* **3**, 995–1000 [CrossRef](#) [Medline](#)
55. Chojnowski, A., Sobota, R. M., Ong, P. F., Xie, W., Wong, X., Dreesen, O., Burke, B., and Stewart, C. L. (2018) 2C-BioID: an advanced two component BioID system for precision mapping of protein interactomes. *iScience* **10**, 40–52 [CrossRef](#) [Medline](#)
56. Franz, C., Walczak, R., Yavuz, S., Santarella, R., Gentzel, M., Askjaer, P., Galy, V., Hetzer, M., Mattaj, I. W., and Antonin, W. (2007) MEL-28/ELYS is required for the recruitment of nucleoporins to chromatin and postmitotic nuclear pore complex assembly. *EMBO Rep.* **8**, 165–172 [CrossRef](#) [Medline](#)
57. Gillespie, P. J., Khoudoli, G. A., Stewart, G., Swedlow, J. R., and Blow, J. J. (2007) ELYS/MEL-28 chromatin association coordinates nuclear pore complex assembly and replication licensing. *Curr. Biol.* **17**, 1657–1662 [CrossRef](#) [Medline](#)
58. Belshaw, P. J., Ho, S. N., Crabtree, G. R., and Schreiber, S. L. (1996) Controlling protein association and subcellular localization with a synthetic ligand that induces heterodimerization of proteins. *Proc. Natl. Acad. Sci. U.S.A.* **93**, 4604–4607 [CrossRef](#) [Medline](#)
59. Fasana, E., Fossati, M., Ruggiano, A., Brambillasca, S., Hoogenraad, C. C., Navone, F., Francolini, M., and Borgese, N. (2010) A VAPB mutant linked to amyotrophic lateral sclerosis generates a novel form of organized smooth endoplasmic reticulum. *FASEB J.* **24**, 1419–1430 [CrossRef](#) [Medline](#)
60. Gasteier, J. E., Madrid, R., Krautkrämer, E., Schröder, S., Muranyi, W., Benichou, S., and Fackler, O. T. (2003) Activation of the Rac-binding partner FHOD1 induces actin stress fibers via a ROCK-dependent mechanism. *J. Biol. Chem.* **278**, 38902–38912 [CrossRef](#) [Medline](#)
61. Charneau, P., Mirambeau, G., Roux, P., Paulous, S., Buc, H., and Clavel, F. (1994) HIV-1 reverse transcription. A termination step at the center of the genome. *J. Mol. Biol.* **241**, 651–662 [CrossRef](#) [Medline](#)
62. Chen, C., and Okayama, H. (1987) High-efficiency transformation of mammalian cells by plasmid DNA. *Mol. Cell. Biol.* **7**, 2745–2752 [CrossRef](#) [Medline](#)
63. Atanassov, I., and Urlaub, H. (2013) Increased proteome coverage by combining PAGE and peptide isoelectric focusing: comparative study of gel-based separation approaches. *Proteomics* **13**, 2947–2955 [CrossRef](#) [Medline](#)
64. Cox, J., and Mann, M. (2008) MaxQuant enables high peptide identification rates, individualized p.p.b.-range mass accuracies and proteome-wide protein quantification. *Nat. Biotechnol.* **26**, 1367–1372 [CrossRef](#) [Medline](#)
65. Vizcaino, J. A., Deutsch, E. W., Wang, R., Csordas, A., Reisinger, F., Rios, D., Dienes, J. A., Sun, Z., Farrah, T., Bandeira, N., Binz, P. A., Xenarios, I., Eisenacher, M., Mayer, G., Gatto, L., et al. (2014) ProteomeXchange provides globally coordinated proteomics data submission and dissemination. *Nat. Biotechnol.* **32**, 223–226 [CrossRef](#) [Medline](#)
66. Carpenter, A. E., Jones, T. R., Lamprecht, M. R., Clarke, C., Kang, I. H., Friman, O., Guertin, D. A., Chang, J. H., Lindquist, R. A., Moffat, J., Golland, P., and Sabatini, D. M. (2006) CellProfiler: image analysis software for identifying and quantifying cell phenotypes. *Genome Biol.* **7**, R100 [CrossRef](#) [Medline](#)